Research Article | Vol. 25, No. 9 | 1 May 2017 | OPTICS EXPRESS 9587

Optics EXPRESS

Plasmon-less surface enhanced Raman spectra induced by self-organized networks of silica nanoparticles produced by femtosecond lasers

YVES BELLOUARD,[1,*] ERICA BLOCK,[1,2] JEFF SQUIER,[2] AND JEAN GOBET[3]

[1]*Galatea Laboratory, IMT/STI, Ecole Polytechnique Fédérale de Lausanne (EPFL), Rue de la Maladière 71b, CH - 2002 Neuchâtel, Switzerland*
[2]*Department of Physics, Colorado School of Mines, Golden, CO, USA*
[3]*CSEM SA, Neuchâtel, Switzerland*
**yves.bellouard@epfl.ch*

Abstract: Raman spectroscopy is the workhorse for label-free analysis of molecules. It relies on the inelastic scattering of incoming monochromatic light impinging molecules of interest. This effect leads to a very weak emission of light spectrum that provides a signature of the molecules being observed. Considerable efforts have been made over the last decades, in particular with the development of Surface Enhanced Raman Spectroscopy (SERS), to enhance the intensity of the emitted signal so that ultimately, traces of molecules can be detected. Here, we show that dense self-organized networks of quasi-monodisperse nanoparticles redepositing during femtosecond laser ablation of trenches in fused silica can lead to a significant field enhancement effect, enabling the Raman detection of a single-molecule layer deposited on the surface (so called monolayer). Unlike previously reported for SERS experiments, here, there is no metal layer promoting plasmonics effects causing localized field enhancement. The method for producing SERS substrates is therefore quite straightforward and low cost.

OCIS codes: (140.7090) Ultrafast lasers; (160.2750) Glass and other amorphous materials; (160.6030) Silica; (180.5655) Raman microscopy; (240.6695) Surface-enhanced Raman scattering.

References and links

1. M. Fleischmann, P. J. Hendra, and A. J. Mcquillan, "Raman spectra of pyridine adsorbed at a silver electrode," Chem. Phys. Lett. **26**(2), 163–166 (1974).
2. M. G. Albrecht and J. A. Creighton, "Anomalously intense Raman spectra of pyridineat a silver electrode," J. Am. Chem. Soc. **99**(15), 5215–5217 (1977).
3. D. L. Jeanmaire and R. P. Van Duyne, "Surface raman spectroelectrochemistry: Part I. Heterocyclic, aromatic, and aliphatic amines adsorbed on the anodized silver electrode," J. Electroanal. Chem. Interfacial Electrochem. **84**(1), 1–20 (1977).
4. S. Nie and S. R. Emory, "Probing single molecules and single nanoparticles by surface-enhanced Raman scattering," Science **275**(5303), 1102–1106 (1997).
5. K. Kneipp, Y. Wang, H. Kneipp, L. T. Perelman, I. Itzkan, R. R. Dasari, and M. S. Feld, "Single molecule detection using Surface-Enhanced Raman Scattering (SERS)," Phys. Rev. Lett. **78**(9), 1667–1670 (1997).
6. J. Kneipp, H. Kneipp, and K. Kneipp, "SERS--a single-molecule and nanoscale tool for bioanalytics," Chem. Soc. Rev. **37**(5), 1052–1060 (2008).
7. M. S. Anderson, "Nonplasmonic surface enhanced Raman spectroscopy using silica microspheres," Appl. Phys. Lett. **97**(13), 131116 (2010).
8. D. Christie, J. Lombardi, and I. Kretzschmar, "Two-Dimensional Array of Silica Particles as a SERS Substrate," J. Phys. Chem. C **118**(17), 9114–9118 (2014).
9. D. Qi, L. Lu, L. Wang, and J. Zhang, "Improved SERS sensitivity on plasmon-free TiO_2 photonic microarray by enhancing light-matter coupling," J. Am. Chem. Soc. **136**(28), 9886–9889 (2014).
10. M. Caldarola, P. Albella, E. Cortés, M. Rahmani, T. Roschuk, G. Grinblat, R. F. Oulton, A. V. Bragas, and S. A. Maier, "Non-plasmonic nanoantennas for surface enhanced spectroscopies with ultra-low heat conversion," Nat. Commun. **6**, 7915 (2015).
11. Y. Nishijima, Y. Hashimoto, L. Rosa, J. B. Khurgin, and S. Juodkazis, "Scaling Rules of SERS Intensity," Adv. Opt. Mater. **2**(4), 382–388 (2014).

#287064 https://doi.org/10.1364/OE.25.009587
Journal © 2017 Received 27 Feb 2017; revised 8 Apr 2017; accepted 10 Apr 2017; published 18 Apr 2017

Optics EXPRESS

12. D. Oron, E. Tal, and Y. Silberberg, "Scanningless depth-resolved microscopy," Opt. Express **13**(5), 1468–1476 (2005).
13. G. Zhu, J. van Howe, M. Durst, W. Zipfel, and C. Xu, "Simultaneous spatial and temporal focusing of femtosecond pulses," Opt. Express **13**(6), 2153–2159 (2005).
14. L. R. Snyder, J. J. Kirkland, and J. L. Glajch, *Practical HPLC Method Development* (John Wiley & Sons, 2012).
15. E. Block, J. Thomas, C. Durfee, and J. Squier, "Integrated single grating compressor for variable pulse front tilt in simultaneously spatially and temporally focused systems," Opt. Lett. **39**(24), 6915–6918 (2014).
16. D. N. Vitek, D. E. Adams, A. Johnson, P. S. Tsai, S. Backus, C. G. Durfee, D. Kleinfeld, and J. A. Squier, "Temporally focused femtosecond laser pulses for low numerical aperture micromachining through optically transparent materials," Opt. Express **18**(17), 18086–18094 (2010).
17. E. Block, M. Greco, D. Vitek, O. Masihzadeh, D. A. Ammar, M. Y. Kahook, N. Mandava, C. Durfee, and J. Squier, "Simultaneous spatial and temporal focusing for tissue ablation," Biomed. Opt. Express **4**(6), 831–841 (2013).
18. R. Kammel, R. Ackermann, J. Thomas, J. Götte, S. Skupin, A. Tünnermann, and S. Nolte, "Enhancing precision in fs-laser material processing by simultaneous spatial and temporal focusing," Light Sci. Appl. **3**(5), e169 (2014).
19. C. G. Durfee, M. Greco, E. Block, D. Vitek, and J. A. Squier, "Intuitive analysis of space-time focusing with double-ABCD calculation," Opt. Express **20**(13), 14244–14259 (2012).
20. J. U. Thomas, E. Block, M. Greco, A. Meier, C. G. Durfee, J. A. Squier, S. Nolte, and A. Tünnermann, "Simultaneously spatially and temporally focusing light for tailored ultrafast micro-machining," Proc. SPIE **8972**, 897219 (2014).
21. D. N. Vitek, E. Block, Y. Bellouard, D. E. Adams, S. Backus, D. Kleinfeld, C. G. Durfee, and J. A. Squier, "Spatio-temporally focused femtosecond laser pulses for nonreciprocal writing in optically transparent materials," Opt. Express **18**(24), 24673–24678 (2010).
22. W. Yang, P. G. Kazansky, Y. Shimotsuma, M. Sakakura, K. Miura, and K. Hirao, "Ultrashort-pulse laser calligraphy," Appl. Phys. Lett. **93**(17), 171109 (2008).
23. B. Poumellec, M. Lancry, J. C. Poulin, and S. Ani-Joseph, "Non reciprocal writing and chirality in femtosecond laser irradiated silica," Opt. Express **16**(22), 18354–18361 (2008).
24. D. Vipparty, B. Tan, and K. Venkatakrishnan, "Nanostructures synthesis by femtosecond laser ablation of glasses," J. Appl. Phys. **112**(7), 073109 (2012).
25. B. W. Kwaadgras, M. W. J. Verdult, M. Dijkstra, and R. Roij, "Can nonadditive dispersion forces explain chain formation of nanoparticles?" J. Chem. Phys. **138**(10), 104308 (2013).
26. B. W. Kwaadgras, R. van Roij, and M. Dijkstra, "Self-consistent electric field-induced dipole interaction of colloidal spheres, cubes, rods, and dumbbells," J. Chem. Phys. **140**(15), 154901 (2014).
27. P. Schapotschnikow and T. J. H. Vlugt, "Understanding interactions between capped nanocrystals: Three-body and chain packing effects," J. Chem. Phys. **131**(12), 124705 (2009).

1. Introduction

Surface Enhanced Raman Spectroscopy since its discovery in the seventies ([1–3]) is based primarily on the use of localized surface plasmons resonant effects ([4,5]) originating from the presence of nanoscale metallic features like for instance, nanoparticles coated with silver or gold. While impressive Raman signal enhancements have been reported (typically from 10^6 to 10^{12}) [4–6], the fabrication of SERS substrates remains complex and costly. Furthermore, the use of metallic nanoparticles poses additional constraints such as their reactivity with the environment being probed, their limited biocompatibility and the lack of reusability [9]. Alternative approaches for Raman enhancement mechanisms are therefore particularly attractive as they may bypass current limitations.

Among the investigated alternative routes, the use of semiconductors, titanium oxide particles, and silica colloids have been proposed. In semiconductors [10], the enhancement mechanism is attributed to a charge transfer between semiconductor particles and the analyte. However, enhancement effects (on the order of 10^3) remain smaller than those obtained with silver or gold nanoparticles. To address this problem, various authors (see for instance [5]) have proposed the use of photonic crystals. Anderson [7] suggested a non-plasmonic method based on a Whispering Gallery Mode (WGM) in isolated micron-size beads of silica. SERS effects have also recently been reported in monodisperse, uncoated, sub-micron silica colloids arranged in 2D crystals [8], although single molecule detection was not achieved. In this case, the enhancement mechanism is attributed to Mie scattering.

Optics EXPRESS

Here we propose yet another alternative Raman enhancement mechanism: a dense network of self-organized, quasi-monodisperse nanoparticles, redeposited during femtosecond laser ablation in fused silica.

2. Methodology

2.1 Production of dense network of nanoparticles

To produce a dense network of nanoparticles, we used a 800 nm Ti:sapphire, chirped pulse amplification (CPA) laser that produced 85 fs pulses at a repetition rate of 1 kHz. The CPA system was equipped with an integrated simultaneous spatial and temporal focusing (SSTF) [11, 12] system as described by Block *et al.* [13].

In this scenario the dispersion compensated pulse is left spatially chirped upon exiting the CPA compressor resulting in increased localization of the intensity at focus, since only there are all spectral components overlapped [14–18]. The degree of an SSTF beam's spatial chirp is described by the beam aspect ratio (the width of the collimated spatially chirped beam relative to the non-chirped beam) in this case ~10. This also determines the degree of pulse front tilt (PFT) present at focus, which has been shown to have an impact on material modifications relative to scan direction [19–23].

The SSTF beam was focused under low numerical aperture conditions (0.05 NA) to a ~20 μm spot (measured $1/e^2$ diameter of the central intensity) on the front surface of a fused silica substrate using a 25.4 mm focal length, 90-degree off-axis parabola. The sample was then translated beneath the focus along the direction of PFT using 3-axis specimen scanning stages. Pulse energies were investigated from 10 to 80 μJ with scan speeds of 1 and 10 mm/s for each pulse energy. These focusing conditions and energy deposition technique allow for an efficient production of nanoparticles. As shown in [24] among others, nanoparticle networks can also be produced by a classical ablation method, i.e. without SSTF.

The fabricated grooves vary from a few microns to a few tens of microns in depth. The ablated material redeposits on both sides of the groove and form intricate networks of nanoparticles as shown in Fig. 1.

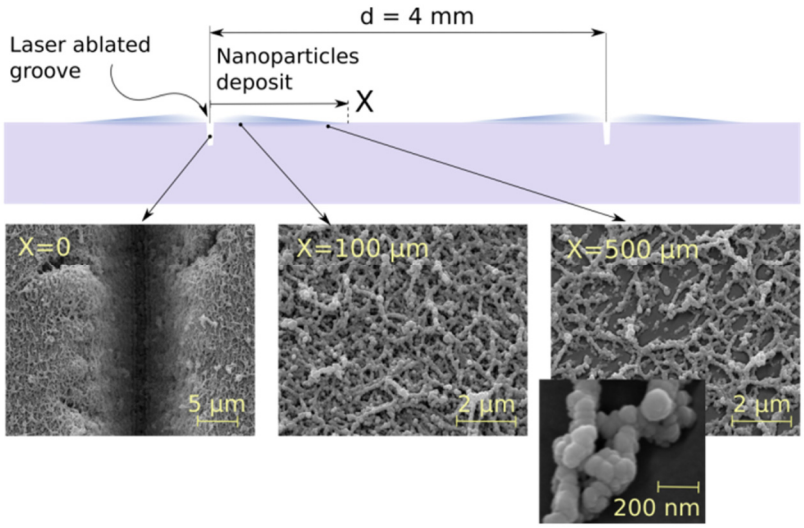

Fig. 1. Laser grooves ablated by a femtosecond laser (at a pulse energy of 40 μJ) using a simultaneous spatial and temporal focusing scheme (SSTF) [11,12]. The distance between grooves is such that no ejecta is found between them. In the deposit region, nanoparticles with typical diameter of slightly less than 100 nm are found. These nanoparticles are not randomly deposited, but spontaneously arrange in planar network assemblies forming layers of decreasing thickness as we move away from the groove.

Optics EXPRESS

2.2 Experimental procedures

The nanoparticle ejecta were coated with polymers according to two procedures.

The first one, in fact found accidently, was through a direct mechanical contact with a stretched polymer membrane (polyurethane) as found in packaging boxes for delicate objects. These membranes are extremely robust and deformable, but through adhesion, it may leave residues on the contacted surface forming a deposit. This procedure is simple and was reproduced multiple times on different specimens. It is however not quantitative, as it is difficult to precisely know what amount of material was deposited. Note that the deposited compounds can be removed by exposing the substrate to a plasma ashing for a few minutes. We refer to this first approach as 'contamination method'.

The second method uses a monolayer deposited through a silanisation process. Technically, we first exposed the substrate to an oxygen plasma activation process for 3 min, and then proceed to a silanisation by exposing the material to a vapor phase of chloro(dimethyl)octylsilane for five hours. The process is terminated by a thermal evaporation step that removes any non-reacted adsorbed molecules. This procedure is known to produce uniform monolayers with a grafting density of 3.2 µmole / m^2 [13].

3. Results

3.1 Contamination by mechanical contact with a polymer membrane

In a first experiment, the substrate was clamped in between two polymer membranes (polyurethane) applying a uniform adhesive force and contaminating the surface as described in the procedures section above. The Raman spectra were taken *after* removing the substrate from the contact of the polymer membranes and by direct observation of the contaminated nanoparticles. The results are shown in Fig. 2. While the spectrum taken in between lines shows the expected peaks for fused silica, the one taken near the trench and within the zones where nanoparticles are found, exhibits a dramatic enhancement. The additional peaks can clearly be attributed to the polymer of the membrane (a reference spectrum taken from the membrane directly is also shown). The spectrum taken in the middle of the trench shows some fainted traces of the membrane spectrum.

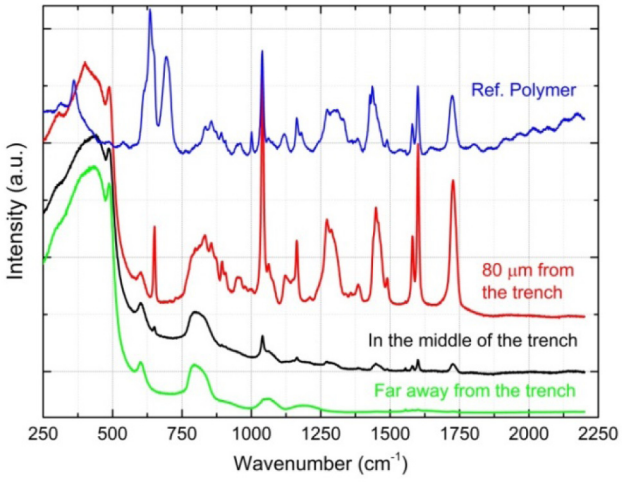

Fig. 2. Raman spectra for a substrate with laser ablated trenches placed in contact with a polyurethane membrane. Starting from the bottom, the curves show the spectra of the substrate measured: 1/ in between lines, 2/ in the middle of the trench, 3/ at a distance of 80 microns from the trench (where nanoparticles are found), respectively. The Raman spectra are normalized using the D1 peak intensity of Silica. The Raman spectrum of the polymer membrane is shown for identification.

Optics EXPRESS

3.2 Monolayer detection

This first experiment shows that an enhancement mechanism is observed in the region where nanoparticle deposits are found. However, the method through direct mechanical contacting does not allow for quantitative evaluation of the enhancement sensitivity. In a second experiment, a monolayer of chloro(dimethyl)octylsilane was deposited in a vapor phase on a substrate of fused silica containing laser ablated trenches, obtained with similar conditions as the previous one. The result shown in Fig. 3, confirms that the substrate with laser ablated trenches is indeed capable of detecting a single molecule layer deposited on the surface.

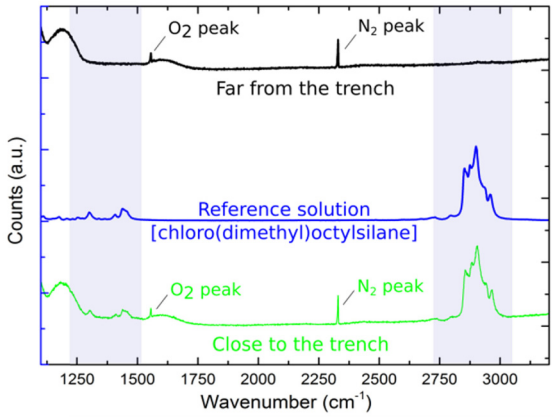

Fig. 3. From bottom to top: Raman spectra taken 1/ at a distance of 30 microns from a trench, 2/ from the reference solution (chloro(dimethyl)octylsilane) used to produce the monolayer and 3/ far from a trench. Peaks attributed to the atmosphere surrounding the specimens are indicated. The two spectra of fused silica were normalized and obtained following rigorously the same measurement procedure. Zones of particular interest are painted in light blue.

3.3 Effect of nanoparticles density and distribution

To test the stability and repeatability of the process, we applied the same preparation procedures on two different specimens, produced at two different periods of time and coated with the same monolayer. On the two specimens, we took a series of Raman spectra around the band 2750-3250 cm^{-1} at increasing distances from the laser trench as well as across the thickness of the deposited layer.

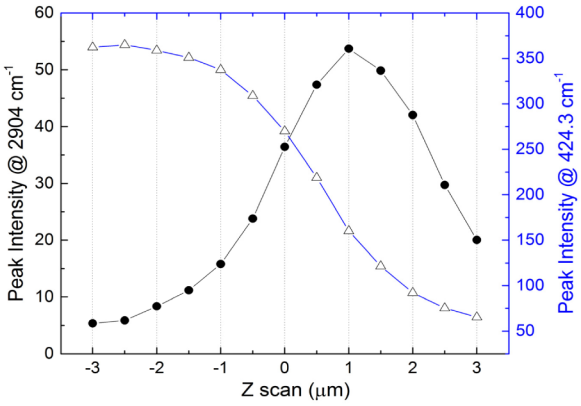

Fig. 4. Raman scan across the surface, illustrating the Raman enhancement and revealing the monolayer is only confined to the nanoparticle layer. The dark dots (left axis) represent the peak intensity of the highest intensity Raman peak of the monolayer. The triangles (right axis) are the peak intensity for the main band of silica.

Optics EXPRESS

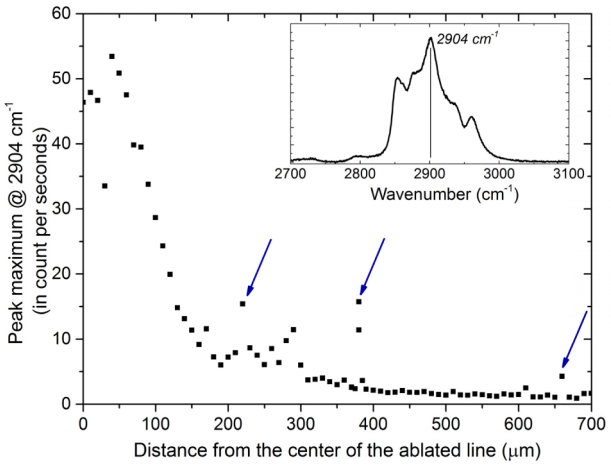

Fig. 5. Raman intensity peak taken at 2904 cm^{-1} (i.e. the most intense peak from the monolayer Raman signal) as a function of the distance from the trench. Measurements were taken every ten microns. The curve shows discontinuity and a few peaks are clearly visible (highlighted with a blue arrow). These peaks are not measurement artefacts and are effectively present. These strong discontinuities suggest the presence of 'hot spots'.

The results are shown in Figs. 4 and 5, specifically comparing the intensity of the peak measured at 2904 cm^{-1} – the most prominent one among the specific peaks related to the monolayer. Both curves show the same behavior and same decay as we move the Raman probe away from the nanoparticle networks. In addition, Fig. 5 shows the presence of sharp peaks (for instance at distance of 225 μm, 375 μm, and 660 μm as indicated by blue arrows). The Raman spectrum was re-measured multiple times to exclude possible measurement errors and consequently yielded the same results. These peaks are therefore not artifacts.

To further verify the possible existence of 'hot spots', we conducted Raman mapping experiments over an 8 x 8 μm area, at a distance of 50 microns from the trench, and then further away at a distance of 400 microns. The results are shown in Fig. 6. These maps are made by acquiring a matrix of Raman scans at points, spaced in both directions by 0.5 micron. Despite the monolayer being deposited on the silica nanoparticles, there is no visible enhancement for the Raman signal coming from the silica molecules themselves. This observation is highlighted in Fig. 7 and suggests that the enhancement mechanism is, as expected, predominantly a surface effect caused by the nanoparticles.

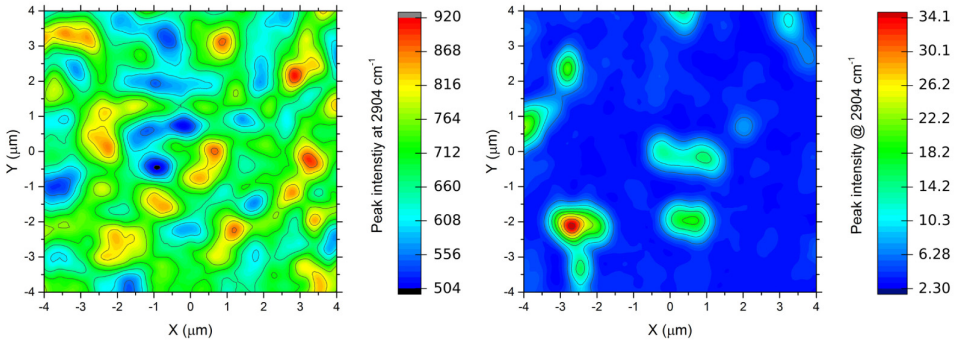

Fig. 6. Raman intensity maps revealing the presence of 'hot spots' where the field-enhancement is the most prominent. Right and left maps are taken at 50 μm and 400 μm from the trench out of which the nanoparticles were expelled (the size of the maps are identical). Parameters for the Raman measurements are rigorously identical for each point and for both maps.

Optics EXPRESS

In this experiment, both Raman signals were acquired in rigorously identical conditions, but at two different locations on the substrate where nanoparticles are present (30 microns from the trench) and far away, where no nanoparticles are to be found (700 microns from the trench).

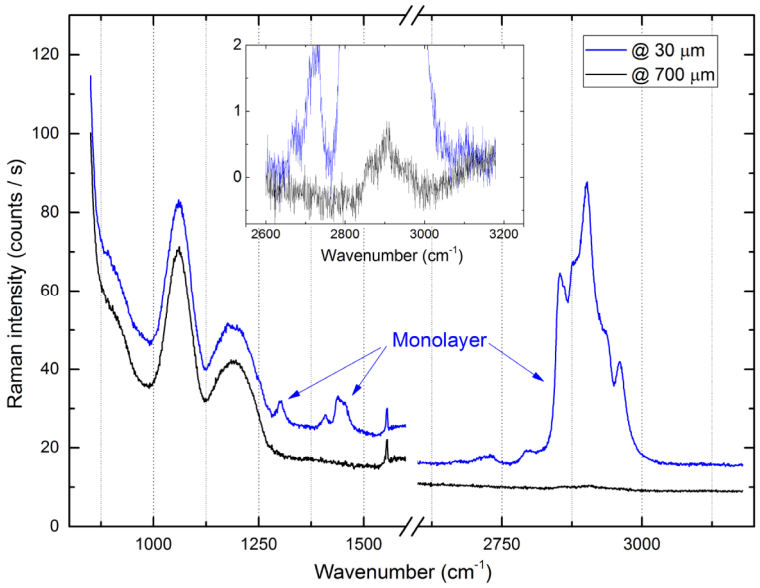

Fig. 7. Two Raman spectra taken at distances close (30 µm) and far away (700 µm) from the trench. Although the monolayer is present everywhere, the enhancement effect affects only the signal of the monolayer deposited on the nanoparticles. The two curves are obtained with rigorously the same Raman exposure and signal collection conditions. The blue curve is arbitrary shifted up for clarity. Inset: Magnified view of the two normalized curves around 2904 cm^{-1}, showing this peak barely visible in the region without nanoparticles (dark curve). We use the intensity ratio for this peak measured at 30 and 700 µm as a rough estimate of the enhancement factor, here between 100 and 150.

4. Interpretation

Let us now discuss the possible mechanism responsible for the local field enhancements. A first hypothesis is to suspect that the monolayer (that was deposited in a vapor phase) may have redeposited and formed a uniform layer everywhere, and on each nanoparticle layer. The large quantities of nanoparticles expelled from the trench offers an increased surface area for molecules to deposit and therefore, logically a larger quantity of molecules is to be found in the vicinity of the trench, and therefore an enhanced Raman signal, not only because of the larger number of molecules present, but also through multiple Mie scattering events.

Two observations contradict this first hypothesis. In our first experiment, we contacted the surface with a polymer through a mechanical interaction (the deposited material was not in a vapor phase). Therefore, only upper nanoparticles in direct physical contact with the membrane are preferably ‘contaminated’. This suggests that the hypothesis of increase volume of particles would not be applicable in this case, unless homogeneous diffusion took place after. However, in two Raman measurements taken with an increased numerical aperture (NA) (not shown here), we observed that the peaks related to the foreign material increase substantially relatively to the host material peaks. As the volume under observations is smaller in the case of a higher NA, one would have expected a lowering of the polymer peaks relative to the peaks of the host substrate. This point further contradicts the argument for a simple surface increase as the main factor for an enhanced Raman signal and suggests another SERS mechanism.

Optics EXPRESS

Nevertheless, this observation does not exclude scattering of the probe Raman light as the main mechanism causing the enhancement. Figures 5 and 6 show some evidences against a pure scattering origin of the effect. Indeed, while doing a systematic scanning of Raman signal moving away from the trench out of which the nanoparticles were extracted, we observed mainly – and as expected – a decay of the Raman peak intensity, but with the presence of localized enhanced peaks, found at random locations (for instance at 225 and 375 μm in the example shown in Fig. 5 and in the form of 'hot spots' in Fig. 6).

To explain this phenomenon, we draw the reader's attention to the fact that the nanoparticles ejected during ablation (of size in the range of 100 nm or less) do not form completely random deposits of decreasing thickness as we move away from the ablation site. As can be seen in Fig. 1, nanoparticles do self-assemble in self-organized structures formed of linear clusters of nanoparticles, eventually forming intricate ring-like and sticks of tens of nanoparticles, much like a net.

The preference for dielectric colloids to self-assemble in linear clusters or alike has been theoretically predicted in [25–27]. In this study, using the couple dipole method (CDM), the authors modeled the nanoparticles as built up out of atoms and took into account all their many-body interactions to study configurations of single atoms, spherical and cube-shaped atomic clusters. They found that the many body van der Waals interactions privileged the formation of linear chains over triangular assembly, in particular if steric interactions exclude triangular assembly, as suggested in [26]. Certainly, the formation of the cluster in the case studied here is a complex problem, including some dynamics aspect and possible charging mechanism during ablation. However, these works [25–27] hint at why such self-organization may take place with dielectric nanoparticles, and form part of an explanation of why nanoparticles expelled during ablation are not randomly depositing. When excited by the laser during the Raman measurement, this self-organized network may form resonating elements (albeit with rather low efficiency) and 'hot spots' (as highlighted in Fig. 6 that supports this hypothesis), enough to create a significant SERS effect, making a monolayer of molecules detectable.

5. Conclusion and outlook

Using femtosecond laser ablation applied to a silica substrate, we have been able to produce a dense network of nanoscale particles that self-organize into semi-structured networks. We attribute this self-organization process to the dipolar coupling between nanoparticles at the time they are expelled from the substrates. Interestingly, we observe that these networks induce a surface enhancement of Raman signals and *de facto* form a so-called SERS substrate. Due to the nature of the nanoparticles (SiO_2), the enhancement effect here cannot be attributed to a plasmonics effect. The localized enhancement effect is instead seen as a consequence of the formation of self-organized chained nanoparticle networks, that once excited by the laser that stimulate Raman emission, create 'hot-spots' (as experimentally shown in this work) leading to a surface field enhancement. All in all, we demonstrated that femtosecond ablation of fused silica substrates offers a very simple and scalable method for producing SERS substrates that are cost-effective, inert, and that can be reused multiple times. The enhancement effect offers sufficient contrast for a clear identification of single layers of molecules as demonstrated here with a layer of chloro(dimethyl)octylsilane.

Funding

European Research Council (ERC-2012-StG-307442)

Acknowledgments

The Galatea Lab further acknowledges the sponsoring of Richemont International SA. We thank Olivier Martin for his valuable suggestions and Christian Santschi for the additional spectrometric measurements.